

# Steady-state frictional sliding contact on surfaces of plastically graded materials

A. Prasad<sup>a,1</sup>, M. Dao<sup>b</sup>, S. Suresh<sup>b,\*</sup>

<sup>a</sup> Department of Civil and Environmental Engineering, Massachusetts Institute of Technology, Cambridge, MA 02139, USA

<sup>b</sup> Department of Materials Science and Engineering, Massachusetts Institute of Technology, 77 Massachusetts Avenue, Cambridge, MA 02139, USA

Received 5 September 2008; received in revised form 23 September 2008; accepted 24 September 2008

Available online 18 November 2008

## Abstract

Tailored gradation in elastic–plastic properties is known to offer avenues for suppressing surface damage during normal indentation and sliding contact. In tribological applications, sliding contact analysis provides a more representative mechanism for fundamental understanding and design as it offers a tool to test materials under conditions of controlled abrasive wear. However, no such study exists for plastically graded materials, although the sliding behavior for elastically graded materials has been reasonably well understood. This study has established a systematic methodology to quantify the mechanics of steady-state frictional sliding response for a plastically graded material. Specifically, the effect of linear gradient in yield stress on the frictional sliding response is examined through parametric finite-element (FEM) computation of the instrumented scratch test. Gradients in yield strength affect both the load carrying capacity of the surface and its pile-up around the sliding indenter. An increase in yield strength with distance beneath the surface shifts the peak values of von Mises stress below the surface, thus improving the resistance of the surface to onset of plasticity and damage. For a given elastic–plastic property, an increasing yield strength gradient causes a reduction in total apparent friction through a reduction in the ploughing coefficient. The contact-load-bearing capacity of plastically graded surfaces follows a similar trend during indentation and scratch. However, significant differences between the pile-up and the friction response are observed between normal indentation and steady-state frictional sliding. In particular, an increase in interfacial friction is found to cause an increase in pile-up during scratch, while it causes a decrease in pile-up during indentation. The implications of the present results to the design of graded surfaces are discussed. © 2008 Acta Materialia Inc. Published by Elsevier Ltd. All rights reserved.

**Keywords:** Plastically graded material; Scratch test; Finite element method; Tribology; Pile-up

## 1. Introduction

Damage-resistant surfaces are required in many engineering components to meet demanding performance requirements in contact applications. For example, in rock drilling equipment, constant rubbing action of the drilling head against the hard surfaces of rocks leads to wear and requires frequent replacement of the drilling head [1]. In Micro-Electro-Mechanical Systems (MEMS) and devices,

high stresses arising from monotonic or repeated contact at between surfaces of small-volume structures can result in increased tribological damage and wear that could result in loss of electromechanical function of the device [2,3]. These examples illustrate the critical need for new and improved materials and design methods for better wear-resistant surfaces.

The concept of purposely introducing controlled gradients in composition, microstructure and elastoplastic properties of gradation as a possible means for improved material design has been explored for a long time [4–7]. Gradual transitions in microstructure and/or composition are indeed commonly observed in natural materials such as bamboos and shells, and in biological materials such

\* Corresponding author. Tel.: +1 617 253 3320.

E-mail address: [ssuresh@mit.edu](mailto:ssuresh@mit.edu) (S. Suresh).

<sup>1</sup> Present address: Mechanics and Materials, Exponent, Menlo Park, CA 94025, USA.

as bones and teeth. In engineering design, property gradation offers flexible means to control and optimize material response through redistribution of thermal and/or mechanical stress, elimination of defect-nucleating stress concentrations and abrupt stress jumps typically occurring at sharp interfaces [8], and control of local crack driving force [6]. These Functionally Graded Materials (FGMs) have found use as damage-resistant surfaces in such widely different applications as aircraft and space vehicles, armored plates, bulletproof vests, industrial equipment and cutting tools. Due to the practical issue of possible material diffusivity (and hence continual change in microstructure) at

high temperatures, a significant amount of research into the long-term use of graded materials has primarily been directed at low temperature applications, in particular to the study of mechanical gradation for resistance to normal contact deformation and damage [7,9–14].

Forms of mechanical gradation for an elastic–plastic material are depicted in Fig. 1 where the gradient is achieved either through a variation in the elastic Young’s modulus ( $E$ ) or the plastic yield-strength  $\sigma_y$ . These materials are defined here as *Elastically Graded Materials* (EGMs, Fig. 1b) and *Plastically Graded Materials* (PGMs, Fig. 1c), respectively. Significant progress has been made in

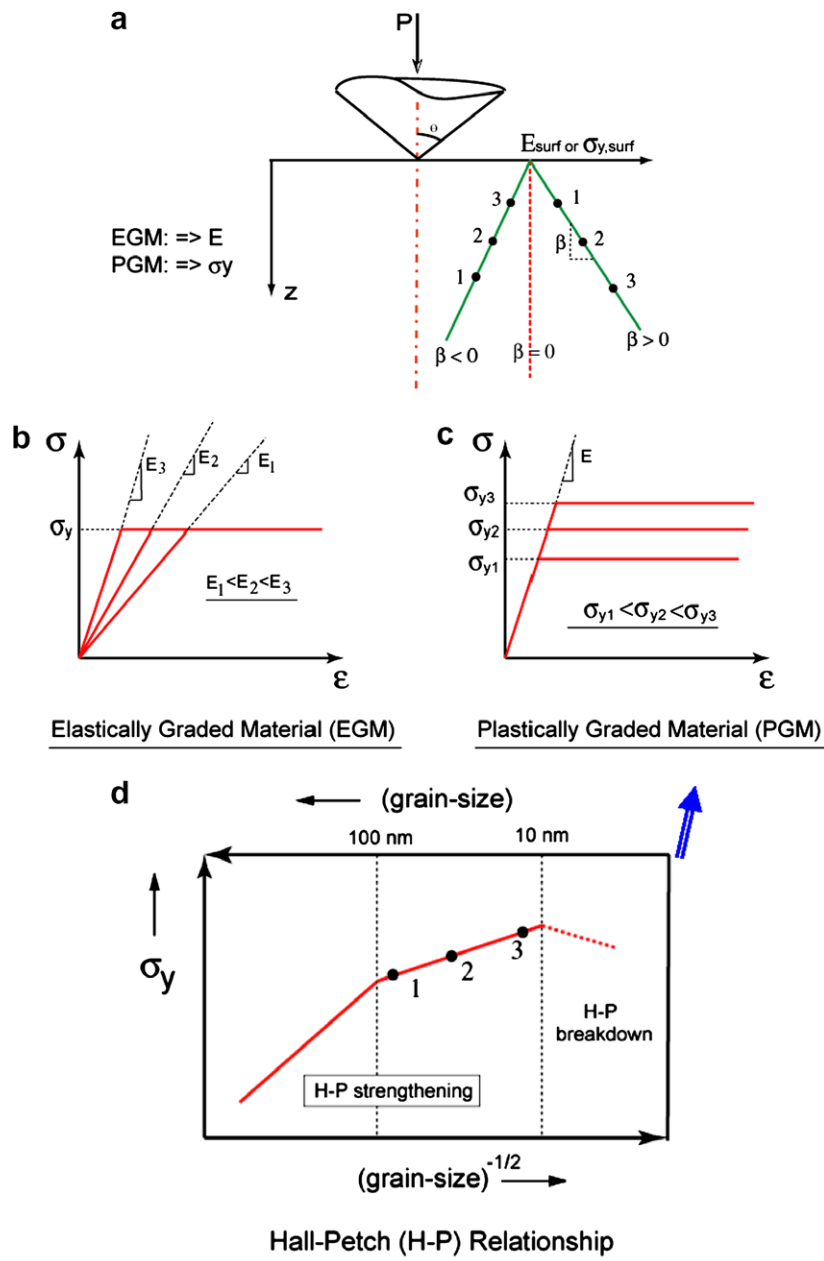


Fig. 1. Mechanical property gradient in elastic–plastic materials (a) Normal indentation on a graded material, the gradient denoted by  $\beta$  where  $\beta > 0$ ,  $< 0$ , and  $= 0$  represents positive, negative and homogeneous materials, respectively. (b) Stress–strain behavior at various locations for elastic gradient. (c) Stress–strain behavior at various locations for plastic gradient. (d) Hall–Petch relationship showing relation between grain-size and yield strength. Points 1, 2 and 3 denote locations for the nano-grained PGM, where the corresponding yield stresses are indicated in (c).

fabricating such controlled microstructure and property gradations over multiple length scales for both EGMs and PGMs. Jitcharoen et al. [9] synthesized EGMs through controlled infiltration of glass into polycrystalline ceramics. Common engineering processes such as shot peening, ion implantation, and case hardening introduce plastic gradient in a controlled manner [6,8]. Another approach to develop plastic gradient is guided by the functional requirements of designing materials with a tunable combination of strength, ductility, and contact-damage resistance. This approach is based on the classic Hall-Petch (H-P) relationship [15,16], together with the superior strength of the nanocrystalline materials (i.e. average grain-size < 100 nm) [17–19]. An example of such an approach is shown schematically in Fig. 1d. Here, a linear gradation in yield strength as a function of depth below the surface can be achieved by increasing (denoted as 3-2-1) or decreasing (denoted as 1-2-3) the grain-size within the nanocrystalline and microcrystalline range through commonly used techniques such as electrodeposition [20]. Such “grain-size graded” nanostructured metals and alloys provide model systems to explore the potential benefits of PGMs for possible tribological applications.

For design of EGMs and PGMs, detailed scientific knowledge of the effects of the microstructure (and mechanical property) gradients on the overall elasto-plastic response under contact conditions is required. Through analytical, computational, and experimental approaches, understanding of the gradient effects in EGMs has been reasonably well achieved for frictionless normal contact. Giannakopoulos and Suresh [7] derived closed-form solutions for contact of point load and axisymmetric indentations with controlled one-dimensional spatially graded EGMs. For this purpose, they considered exponential and power law elastic modulus gradients as functions of depth below the surface, and the indentation load was analyzed as a function of penetration depth for different controlled variations in elastic modulus. These studies revealed that increasing elastic modulus below the surface caused the maximum tensile stress responsible for crack nucleation to shift towards the interior and hence resulting in suppression of surface damage and crack nucleation. In later studies, the theoretical results were validated through finite element simulations as well as well-controlled experimental studies on specially designed EGMs [7,9,10,21]. For experimental validation, model EGMs were designed whereby long-range internal stresses were avoided by careful selection of constituent material and processing method [9,21]. The EGMs with increasing modulus demonstrated higher resistance against development of Hertzian cone cracks in normal contact [7,9,21] and against herringbone cracks in sliding contact [10].

Studies of PGMs began to emerge starting with the work by Suresh [6] and Giannakopoulos [11] who suggested possible approaches for predicting the load-depth response of PGMs under conical indentations. Based on a parametric study using finite element analysis, Cao and

Lu [12] derived dimensional functions for the load-depth response of linear plastic gradients under an equivalent Berkovich indenter. More recently, Choi et al. [13,14] developed closed form universal dimensional functions for generalized depth-sensing instrumented indentation of PGMs under frictionless normal loading, and experimentally verified their predictions for the case of a linear yield-strength gradient. These studies on PGMs demonstrated the benefits of a positive plastic gradient (increasing yield strength beneath the contact surface) on the stress-strain and deformation response in normal indentation.

Despite these advances in fundamental understanding, normal indentation has restricted relevance for predicting the tribological response. The instrumented frictional sliding (scratch) test provides a more realistic tool to test materials under conditions of controlled abrasive wear [22]. It is routinely employed in practice to compare hardness and abrasive resistance of surfaces, to extract information relating to mechanisms of deformation, and to study delamination of coatings [22–24]. Progress in instrumentation now provides the means to experimentally monitor the load versus indenter penetration depth response in normal as well as in frictional sliding contact over large variations in length scales (from nm to  $\mu\text{m}$  scale indenter penetration depths), observe friction evolution through continuous measurement of tangential loads along the scratch, and obtain residual scratch profiles and pile-up/sink-in responses using a high precision profilometer and/or an atomic force microscope. Finite element simulations of the instrumented scratch test require a full three-dimensional analysis because of the lack of symmetry of the loading configuration, except for symmetry with respect to the scratch line. These simulations also require highly refined finite element meshing along the scratch path in order to study the steady-state response. Significant improvements in the computational power now allow for investigation of such large-scale problems with acceptable accuracy. These developments have, however, not been exploited to elucidate the micro- and nanomechanics of frictional sliding of plastically graded materials, although such studies for homogeneous materials have recently been reported [25–27]. The present study thus aims to report systematic results of the tribological response of PGMs through detailed computational simulations of the instrumented, depth-sensing, frictional sliding or scratch test. Such information is of practical value for the design of materials with improved resistance to tribological damage and failure. It is also of fundamental scientific interest to explore the effects of gradients in materials properties on frictional sliding response vis-à-vis the micromechanics of instrumented indentation and frictional sliding of homogeneous materials.

## 2. Background Information

The scratch test is the oldest known form of hardness measurement, its application dating back to 1824 when the Mohs

scale [28] was developed to rank minerals in terms of their scratch resistance. Normal indentation tests were developed almost two decades later by Brinell [29] and Meyers [30]. The physical significance of hardness measurement was first brought to light by Tabor [31] who suggested the following general relation between the indentation hardness ( $H_1$ ) and plastic property of rigid-perfectly-plastic materials

$$H_1 = C\sigma_r, \quad (1)$$

where  $C$  is a constant approximately equal to 3, and  $\sigma_r$  is yield strength at some representative value of strain. Tabor also deduced the ratio of scratch hardness to indentation hardness as 1.2 for metals. Though a much wider range of this ratio, ranging from 1.6 to 0.58, is suggested in later studies [31–34], this result is significant in demonstrating a correspondence between the two measures of hardness.

Recent developments in instrumented indentation techniques provide the ability to measure the load versus depth response continuously across length scales. Additionally, most instrumented indenters can also be used to perform the scratch test; examples include the Nanotest<sup>®</sup> 600 (Micro Materials, Ltd., Wrexham, United Kingdom) and the TriboIndenter (Hysitron Inc., Minneapolis, MN, USA). These advances in instrumentation have been exploited to extract mechanical properties from indentation response, beginning with the work by Oliver-Pharr [35]. Since then, significant progress has been made in characterizing elastic–plastic properties using the indentation load versus penetration depth curves [36,37]. Taking advantage of these developments in instrumentation, experimental studies of the scratch test have also been recently undertaken [25–27]. However, due to the inherent three-dimensionality of the frictional sliding contact problem, limited information is currently available in the literature on the mechanics of the instrumented scratch test.

Hamilton and Goodman [38] derived explicit equations to predict the stress field for the frictional sliding of a spherical indenter on an elastic medium. Simplifying assumptions with regard to either the dimensionality [39–43] or the deformation mechanism [44–46] have been used to arrive at approximate theoretical solutions for elastic–plastic medium. These and other related work [47–50], though limited in practical applications, are significant in identifying key parameters governing deformation during scratch. Bowden and Tabor [47] explained the role of friction through its decomposition into the deformation (adhesive coefficient) and the geometry (ploughing coefficient) terms. The influence of normalized material property  $\frac{E}{\sigma_y}$  and the indenter geometry  $\theta$  was observed in indentation and scratch test [51–53] and the following governing parameter was identified [50]

$$\chi = \frac{E}{\sigma_y} \tan \theta. \quad (2)$$

For  $\chi < 2$ , the response is governed by elastic properties while for  $\chi > 50$  the response is dominated by plastic properties [50].

FEM computation offers an attractive alternative to study the generalized scratch behavior [54,55]. Subhash and Zhang [56] identified the effect of friction on the scratch hardness of homogeneous materials through the investigation of changes in overall friction coefficient as a function of the indenter angle and the interfacial friction. In several recent studies [25–27], the difference in the indentation and scratch mechanism was identified through the representative strain during the scratch test being 33.6%, which is roughly four times higher than during the indentation test defined earlier [31]. These authors also demonstrated a strong influence of friction and strain-hardening ( $n$ ) on the material pile-up along the indenter and hence on the scratch hardness measurement. However, the mechanics of the instrumented scratch test has thus far not been studied in detail.

### 3. Computational model

A number of previous studies have successfully used the finite element method for investigating the mechanics of frictional sliding in homogeneous materials [25–27,54–56]. Here, to study the effect of gradient on the tribological response of PGMs, the scratch test on graded materials is simulated using the commercial FEM package ABAQUS Standard (SIMULIA, Providence, RI, USA).

#### 3.1. Constitutive model

The material is modeled as elastic–plastic, where the elastic behavior is modeled using Hooke’s law (Eq. (3a)) and the plastic behavior using the von Mises isotropic power law strain hardening (Eq. (3b)).

$$\sigma = E\varepsilon, \quad \text{for } \sigma \leq \sigma_y \quad (3a)$$

$$\sigma = R\varepsilon^n, \quad \text{for } \sigma \geq \sigma_y \quad (3b)$$

Here  $E$  is Young’s modulus,  $\sigma_y$  is the initial yield stress at zero offset strain,  $n$  is the strain-hardening exponent;  $R$  is a strength coefficient, and  $\sigma\varepsilon$  are the true stress and strain. Decomposing the strain into the yield and the plastic strain ( $\varepsilon = \varepsilon_y + \varepsilon_p$ ) and applying conditions of continuity at yielding for the two curves of Eqs. (3), the stress–strain equation beyond yield is written as

$$\sigma = \sigma_y \left( 1 + \frac{E}{\sigma_y} \varepsilon_p \right)^n. \quad (4)$$

The nomenclature related to indentation and scratch is depicted in Fig. 2, where

$\theta$	included apex angle of the cone
$z$	depth below surface
$h_m$	maximum <i>in-situ</i> depth
$h_r$	residual depth after unload
$a_m$	“true” contact radius at maximum <i>in-situ</i> depth
$a_r$	contact radius at maximum residual depth
$a$	apparent contact radius at maximum <i>in-situ</i> depth ( $=h_m \tan \theta$ )

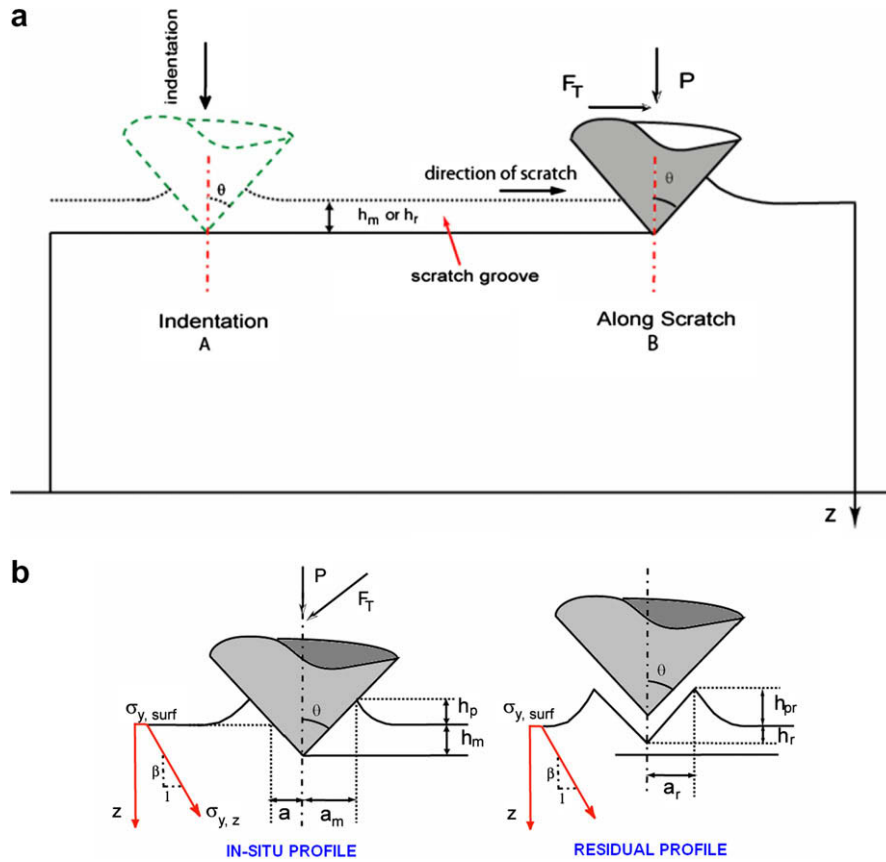


Fig. 2. Schematic of typical indentation and scratch test in an elastic-plastic material and the related geometrical parameters for a conical indenter. (a) Indentation and scratch where the location ‘‘A’’ denotes indentation, followed by sliding along A–B, with ‘‘B’’ denoting the position of the indenter along the scratch. (b) Details of the typical profile perpendicular to scratch in the *in-situ* and residual condition where  $a_m$ ,  $h_m$  denote the terms for the *in-situ* profile and  $a_r$ ,  $h_r$  denote the terms for the residual profile.

$h_p$  *in-situ* pile-up height  
 $h_{pr}$  residual pile-up height

Gradient in the yield strength is introduced along the depth below surface and is characterized by the parameter  $\beta$ . For the linear variation of yield strength with depth, the yield stress at a depth  $z$  below surface can be represented as

$$\sigma_{y,z} = \sigma_{y,surf}(1 + \beta z) \quad (5)$$

where  $\sigma_{y,surf}$  and  $\sigma_{y,z}$  are the yield strength at the surface and at depth  $z$  below, respectively. The external subroutine feature of ABAQUS is used to introduce such a plasticity gradient independent of the mesh design.

### 3.2. Dimensional analysis

Using a sharp conical indenter on a plastically graded material, the mechanical response of frictionless steady-state sliding is found to depend on the material properties, tip geometry and penetration depth:

$$h_p = f_p(E^*, \sigma_{y,surf}, n, \theta, \beta, h_m), \quad (6a)$$

$$P = f(E^*, \sigma_{y,surf}, n, \theta, \beta, h_m), \quad (6b)$$

$$F_T = f_T(E^*, P, \sigma_{y,surf}, n, \theta, \beta, h_m). \quad (6c)$$

Here  $E^*$  is the reduced modulus incorporating Young’s modulus and Poisson’s ratio for the indenter ( $E_I, \nu_I$ ) and surface ( $E, \nu$ ), respectively, and is given by Eq. (7) [57], the other terms are defined earlier.

$$\frac{1}{E^*} = \frac{1 - \nu_I^2}{E_I} + \frac{1 - \nu^2}{E}. \quad (7)$$

Dimensional analysis provides an important tool to handle such large parametric range of analysis, through the reduction of the total number of dimensionless variables. This method has been used to derive universal scaling relations for the indentation and the scratch test on homogeneous and graded materials [13,14,25–27,36]. Here, applying the Pi theorem of the dimensional analysis and using  $\beta h_m$  to represent dimensionless form of the gradient [13,14], the above relations can be reduced to the following general functional forms, with the exact forms of these functions presented later in the paper.

$$\frac{h_p}{h_m} = \Pi_1 \left( \frac{E^*}{\sigma_{y,surf}}, \beta h_m, n, \theta \right), \quad (8a)$$

$$\frac{P}{\sigma_{y,surf} h_m^2} = \Pi_2 \left( \frac{E^*}{\sigma_{y,surf}}, \beta h_m, n, \theta \right), \quad (8b)$$

$$\frac{F_T}{P} = \mu_{app} = \Pi_3 \left( \frac{E^*}{\sigma_{y,surf}}, \beta h_m, n, \theta \right). \quad (8c)$$

### 3.3. Finite element model setup

A full three-dimensional mesh is used in the FEM analysis with the domain boundary chosen sufficiently from the point of indentation so as to circumvent any boundary effects. The overall mesh is shown in Fig. 3a and consists of 97,186 first-order, reduced integration tetrahedral elements. The indenter is modeled as a rigid cone, with an apex angle of  $70.3^\circ$  (considered equivalent to a Berkovich indenter) and is placed asymmetrically along the scratch path. The mesh is refined in the zone of contact such that at least 12 elements are in contact at the end of the initial indentation step. During the subsequent scratch process, the number of elements in contact gradually increases due to the increase in material pile-up along the indenter (Fig. 3b).

Indentation and scratch were simulated respectively by moving the indenter normally to a fixed depth and then tangentially along the scratch direction up to a maximum of approximate six times the contact radius to reach steady state. Large deformation formulation with displacement control steps is used. Numerical convergence becomes increasingly difficult with increasing material plasticity. Hence, for highly plastic materials, a gradually decreasing scratch depth was used for the first one-third of the total scratch length, while keeping the scratch depth constant beyond that. This has been observed to result in faster convergence, as it partly overcomes the initial “softening effect” in load due to decreased area of contact. The implicit analysis scheme of ABAQUS/Standard is used for analysis as it allows for comparative ease in simulating property gradient.

The FEM model setup and basic results are validated by comparisons with previously known theoretical and numerical solutions for select or limiting cases. In particular, the FEM result was compared against the theoretical solution of frictional sliding of a spherical indenter on uniform elastic material [38]. The result is found to be within 2% of the theoretical solution for an adhesive frictional coefficient  $\mu_a < 0.25$ , and within 11% for  $\mu_a = 0.50$ . The

increased deviation at higher friction is due to the simplified assumption regarding contact pressure distribution in the earlier analytical study [38]. The normal indentation response of elastic-plastic materials is found to be in close agreement with the closed form solutions of Dao et al. [36]. Finally, the integration of the external subroutine has been verified by reproducing previously published results for the normal indentation of elastic and plastic gradients [7,13].

## 4. Results and discussion

Frictionless scratch simulations are performed for a range of material properties representing common engineering metals. The Young’s modulus  $E$  is varied from 10 to 200 GPa and the surface yield strength  $\sigma_{y,\text{surf}}$  is varied from 10 to 3000 MPa such that  $E/\sigma_{y,\text{surf}}$  varies uniformly from 40 to 500; the fixed material parameters are the Poisson’s ratio of 0.3 and the strain-hardening exponent of 0.1. The choice of the hardening exponent in this parametric study is guided by the low hardening of nanocrystalline and ultra-fine grained metals and alloys which are candidate materials for practical applications involving PGMs. Five different values of plasticity gradient are considered (i.e.,  $\beta h_m = 0.0, 0.25, 0.5, 1.0$  and  $1.25$ ), resulting in a total of 60 different cases. A limited number of additional simulations are carried out to study the effect of friction on PGMs ( $\mu_a = 0.0, 0.08$ , and  $0.12$  for  $\beta h_m = 0.0$  and  $0.5$  and  $E^*/\sigma_{y,\text{surf}} = 137.4$ ).

### 4.1. Pile up response and strain field

During normal indentation of elastic-plastic materials, pile-up or sink-in is observed whereby the material is either pushed up outward along the indenter or down inward towards the bulk material, respectively [48]. This causes deviation of the apparent contact area from the true contact area and hence can lead to significant errors in hardness measurements [58]. The amount of pile-up is further amplified during the scratch test [25,55]. Knowledge of material pile-up and sink-in is necessary to gain a complete under-

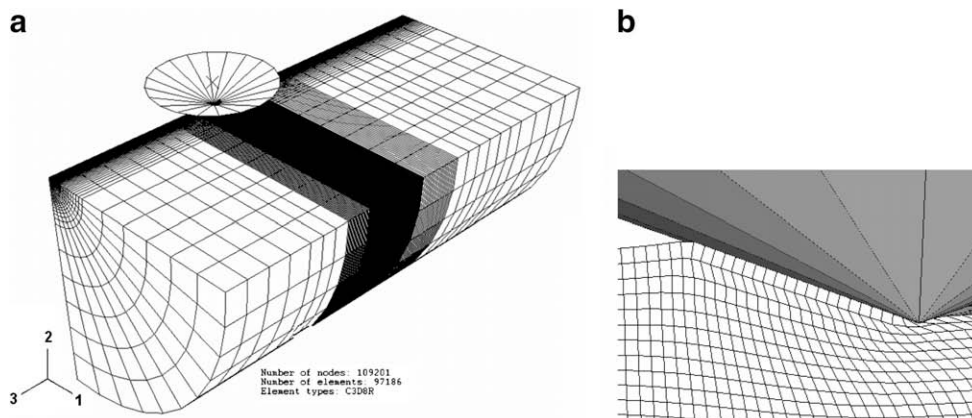


Fig. 3. Overall mesh design with conical indenter for scratch simulation (a), with details of mesh close to the indenter at full contact (b). The scratch direction is along the negative “3” direction in the figure.

standing of the mechanics of contact and to estimate material properties from instrumented contact experiments.

For homogenous materials, the pile-up behavior is a function of material property  $E^*/\sigma_y$  and strain-hardening exponent  $n$  [59]. A similar trend is also observed in the current study, where the normalized pile-up increases with an increase in  $E^*/\sigma_{y,surf}$  as shown in Fig. 4. For a given  $E^*/\sigma_{y,surf}$ , however, the normalized pile-up response increases initially for a lower value of gradient, gradually changing to a decreasing trend at steeper gradients (Fig. 5a). Overall, the pile-up appears to be a stronger function of surface property  $E^*/\sigma_{y,surf}$  than of the plastic gradient term  $\beta h_m$ . Also shown in Fig. 5a is the dimensionless equation for the pile-up behavior which is discussed later in Section 4.6.

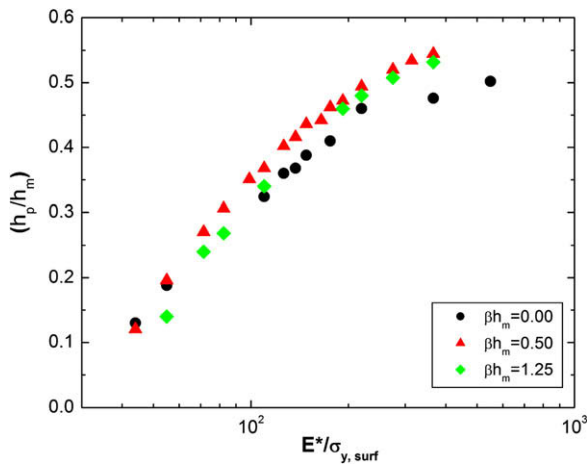
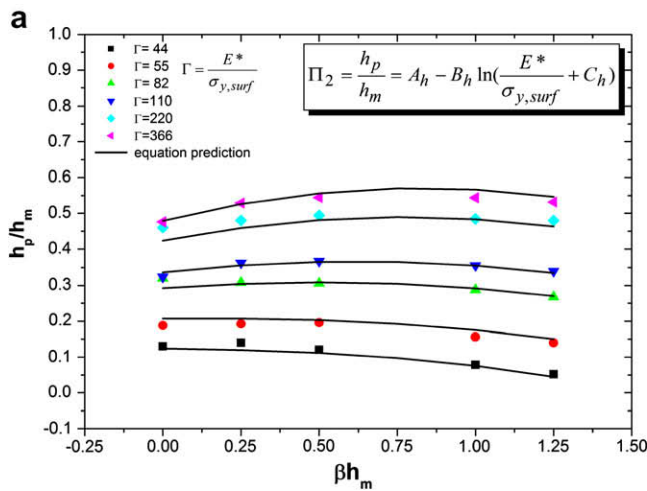


Fig. 4. Variation of normalized *in-situ* pile-up at steady state scratches with material parameter for homogeneous and graded materials ( $\beta h_m = 0.50, 1.25$ ). For both, for the homogeneous and graded materials, the pile-up responses show a strong influence of material parameter  $E^*/\sigma_{y,surf}$  with the pile-up increasing with an increase in  $E^*/\sigma_{y,surf}$ .



The observed pile-up trend, though not intuitively obvious, is a result of the distribution of plastic strains below the indenter (Fig. 5b). The zone of plastically strained material lies within approximately twice the scratch depth from the top surface. As indicated in Fig. 5b, gradient in yield-strength causes an increase in the surface plastic strain distribution together with a decrease in the depth of plastically strained zone. Due to the localized nature of plastic strain, the pile-up response appears to be a strong function of the surface property. For a steeper gradient, however, the increased strain is partly counteracted by the higher strength material closer to the surface, leading to the decreasing trend in the pile-up. An increase in the *in-situ* pile-up was also observed for indentation on PGMs [13,14], although at much higher gradient reflecting the difference in deformation modes of the indentation test and scratch test (namely localized compression and surface shearing, respectively).

#### 4.2. Normal load capacity and stress field

In contrast to the pile-up behavior, the normalized loading response is significantly affected by the increase in plasticity gradient as shown in Fig. 6a. Here, the effect of gradient becomes increasingly prominent at higher  $E^*/\sigma_{y,surf}$  ratios (also shown in the figure are the curves predicted using the dimensionless functions described in Section 4.6). A similar trend is also expected from the increase in the strain-hardening exponent for homogeneous materials. However, the difference in the underlying mechanism of homogeneous and plastically graded materials can be seen from Fig. 6b where typical von Mises stress is plotted for three different gradients ( $\beta h_m = 0.0, 0.50,$  and  $1.25$ ), at a vertical line ahead of the indenter along the scratch direction. For homogeneous materials ( $\beta h_m = 0.0$ ), the highest stress zone lies close to the surface.

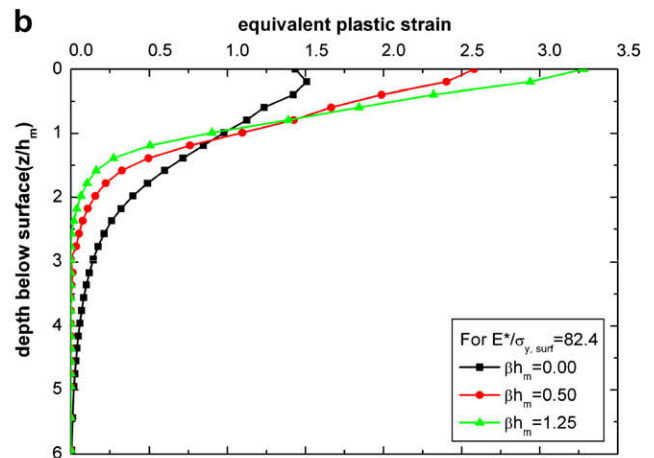


Fig. 5. (a) Variation of normalized *in-situ* pile-up with gradient and (b) typical equivalent plastic strains across depth below indenter ( $E^*/\sigma_{y,surf} = 82.4, \beta h_m = 0.0, 0.5,$  and  $1.25$ ). Pile-up initially increases with an increase in gradient and then starts to decrease for higher gradients. The strain profile can be used to explain this phenomenon through relatively small zone of plastically strained material below indenter. Also shown in (a) is the dimensionless equation prediction for which the details are discussed later in Section 4.6.

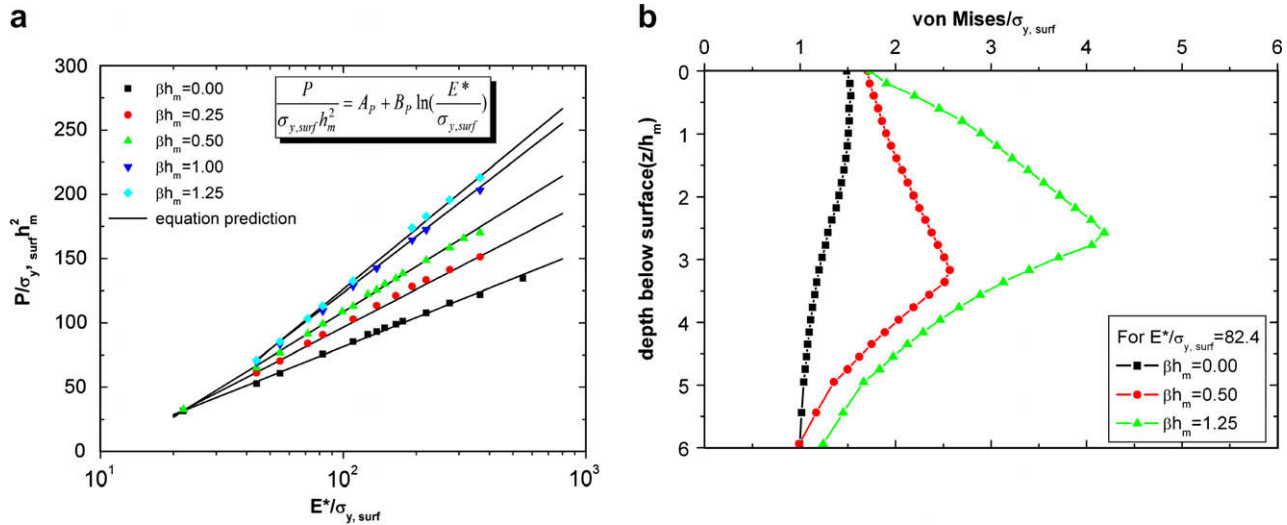


Fig. 6. Details of steady state loading response showing (a) variation in normalized load with respect to  $\beta h_m$  and (b) typical von Mises stresses versus depth, ahead of the indenter along the scratch direction ( $E^*/\sigma_{y,surf} = 82.4$ ,  $\beta h_m = 0.0, 0.5, 1.25$ ). The increased load for graded materials is attributed to the redistribution of higher stressed zone below surface. The zone of influence of gradient appears to be within five times the indentation depth. Also shown in (a) is the dimensionless equation prediction, the details of which are discussed later in Section 4.6.

In contrast, for PGMs, redistribution of stresses occurs such that while the surface stress remains roughly the same, the zone of maximum stress shifts below the surface. The affected zone of plasticity gradient appears to be within approximately five times the scratch depth.

4.3. In-situ scratch hardness

In line with the traditional definition of hardness [31], the *in-situ* scratch hardness here is based on the area defined by half the circle of contact radius  $a_m$  (see Fig. 2 for nomenclature) and is given by,

$$H_{S,in-situ} = \frac{2P}{\pi a_m^2}. \tag{9}$$

This hardness measure incorporates the effect of the trends in the pile-up and the load capacity and is shown in Fig. 7a. (The scatter in the hardness data is due to the scatter associated with the estimation of the pile-up. In order to get an exact value of the pile-up from simulation, a node should be exactly at the tip of the pile-up, which is usually not achieved even with the refined finite element mesh).

From previous studies of the scratch test on homogeneous materials [25–27], a representative strain in the range of 33.6–35% was identified for normalized hardness of materials with low strain-hardening. In the current study, an additional length scale is necessary due to the plasticity gradient. To incorporate that in the context of a representative strain, a “representative depth” is introduced and is

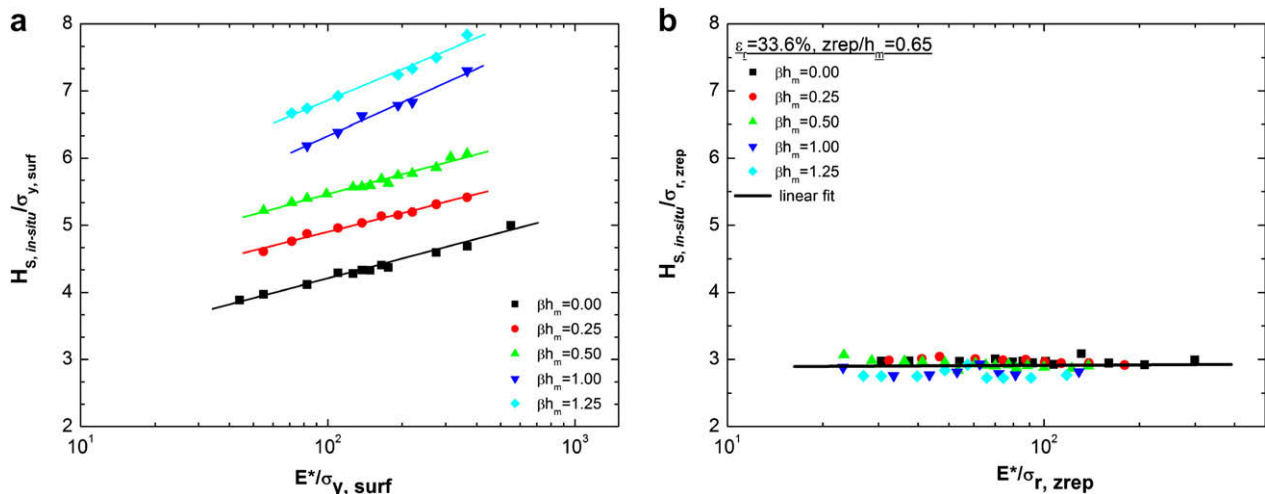


Fig. 7. (a) Variation of *in-situ* hardness with material parameter for  $\beta h_m = 0.0, 0.25, 0.50, 1.0, 1.25$  and (b) normalized hardness value using a representative strain of 33.6% and a representative depth of  $0.65h_m$ .

defined as “the depth below surface, at which the yield stress denoted by  $\sigma_{y,zrep}$  can be used to characterize the normalized scratch hardness, independently of the material gradient”. Using a representative strain of 33.6%, a representative depth of  $0.65h_m$  can be obtained empirically, at which the curves of Fig. 7a collapse to a single curve within 5% error (Fig. 7b). The hardness of the graded surface can then be expressed as

$$\frac{H_{S,in-situ}}{\sigma_{r,zrep}} = 2.87 + 0.009 \ln \left( \frac{E^*}{\sigma_{r,zrep}} \right). \quad (10)$$

The foregoing definition of hardness is based on the *in-situ* area of contact. In the depth-sensing indentation test, *in-situ* hardness can be estimated relatively easily using detailed analyses [36,37]. However, in absence of such schemes for the scratch test, the experimental scratch hardness measure is based on the residual area of contact. The difference between the *in-situ* and residual hardness will depend on the elastic recovery at the profile diameter, an estimate of which has not been made in this study. However, based on earlier studies [11,60], these two hardness measures are expected to be close, especially for materials having significant plasticity. More importantly, the overall trend observed in Fig. 7a is expected to remain unchanged by elastic recovery for this class of materials.

#### 4.4. Effect of friction

The apparent friction coefficient ( $\mu_{app}$ ) is given by the ratio of the tangential force ( $F_T$ ) to the normal force ( $P$ ). It can be further decomposed into the adhesive ( $\mu_a$ ) and ploughing ( $\mu_p$ ) terms [47] as

$$\mu_{app} = \frac{F_T}{P} = \mu_a + \mu_p. \quad (11)$$

For a sharp conical indenter of apex angle  $\theta$ , under the assumption of constant contact pressure and full elastic recovery in the wake of the indenter, the ploughing friction term is written as

$$\mu_p = \frac{2}{\pi} \cot \theta. \quad (12)$$

Fig. 8 shows the ploughing friction coefficient from the frictionless scratch simulation (i.e.  $\mu_a = 0$ ). Both for homogeneous and graded materials, the value of the ploughing friction coefficient increases with the increase in  $E^*/\sigma_{y,surf}$ , gradually approaching the theoretical prediction of Eq. (12) for higher  $E^*/\sigma_{y,surf}$ . The deviation from the theoretical value is a result of the simplified assumptions used in the derivations, which are obeyed closely only at higher values of  $E^*/\sigma_{y,surf}$ .

It is also observed that for a given  $E^*/\sigma_{y,surf}$ , an increase in the gradient causes a decrease in the ploughing term. This is of significance in tribological applications where reducing friction even by small amount can result in large improvements in the wear response [39]. Based on earlier discussions in Sections 4.1 and 4.2, this decrease in friction for the graded system can be attributed to the increase in normal load capacity without a comparable change in the material pile-up response.

Fig. 9 shows the stress and strain plots from the frictional sliding simulation, at a vertical line ahead of the indenter along the scratch direction. The stress distribution shows little sensitivity to the changes in friction. However, increase in the interfacial friction results in increased

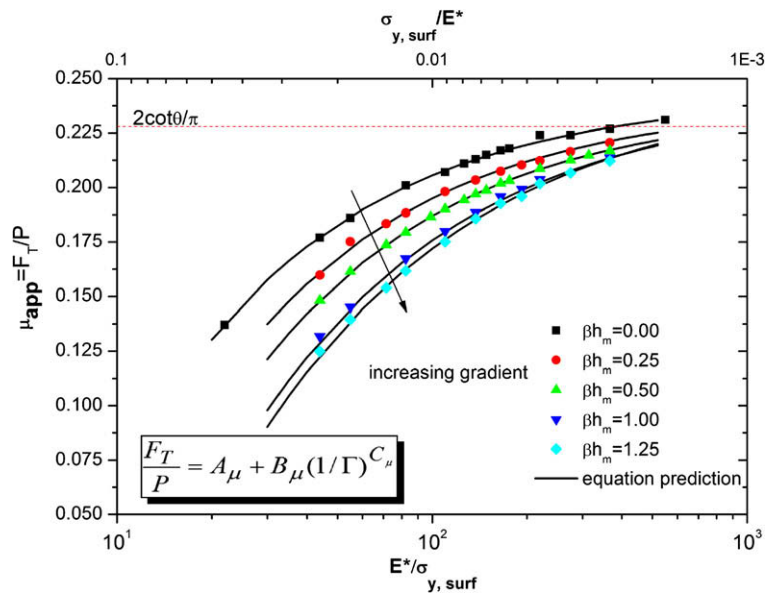


Fig. 8. The effect of material property on apparent friction coefficient from frictionless scratch simulation ( $\mu_{app} = \mu_p$ , for  $\mu_a = 0$ ). The homogeneous case approaches the theoretical value of “ploughing friction” for material with high plasticity. Increasing gradient causes a decrease in the apparent friction coefficient due to the increasing normal load, with relatively small variation in the pile-up. Also shown in the figure is the dimensionless equation prediction for the material cases considered, details of which are discussed later in Section 4.6.

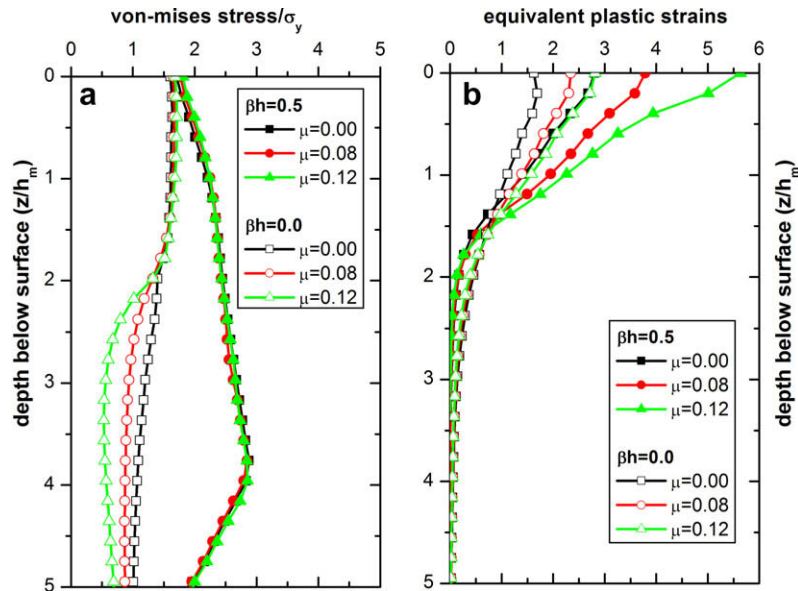


Fig. 9. Effect of changes in friction coefficient ( $\mu_a = 0.0, 0.08$ , and  $0.12$ ) on (a) the von Mises stress and (b) the equivalent plastic strain below indenter. The location and value of the maximum stress shows relative insensitivity to friction; while the plastic strains on the surface increases, causing an increase in the pile-up height.

surface plastic strains, which translate into increased pile-up response as shown in Fig. 10.

#### 4.5. Indentation versus scratch measurements

This section briefly summarizes the differences in the trends observed between the indentation and frictional sliding (scratch) tests. Fig. 11a shows trends in the loading response for homogeneous and graded materials from indentation and sliding simulations. Both tests show similar trends in behavior, with the load in a scratch test approximately 10% higher than that in an indentation test.

However, there is a 2- to 3-fold increase in the pile-up response during scratch, as shown in Fig. 11b for two different values of  $E^*/\sigma_{y,surf}$ , where the open symbols are for indentation and filled symbols are for scratch. In addition, friction tends to increase pile-up in a scratch test while it decreases pile-up in an indentation test (Fig. 10). Overall, from the frictionless scratch simulations, the ratio between the scratch and indentation hardness is observed to be in the range of 1.2–1.6 (Fig. 12), whereas the indentation hardness is defined as

$$H_{I,in-situ} = \frac{P}{\pi a_m^2}. \quad (13)$$

Although the indentation and the scratch test responses are both guided by the plastic properties of the material, there lie significant differences between the two. These differences are due to the differences in the deformation modes and the level of plastic straining. In practice, the indentation test is preferred than the scratch test due to the relative ease in conducting experiments and performing quantitative simulations, and in interpretation of the analysis results. There is thus an obvious advantage in drawing a clear correlation between the two tests such that material response from one can be inferred to interpret behavior in the other case.

#### 4.6. Prediction of sliding response

Based on the above parametric FEM analysis of the sliding contact for PGMs, the following functional forms for the dimensional functions  $\Pi_1$ ,  $\Pi_2$  and  $\Pi_3$  are constructed by first selecting a suitable functional form and then best-fitting the FEM results from a large number of simulations to obtain the analytical expressions detailed below.

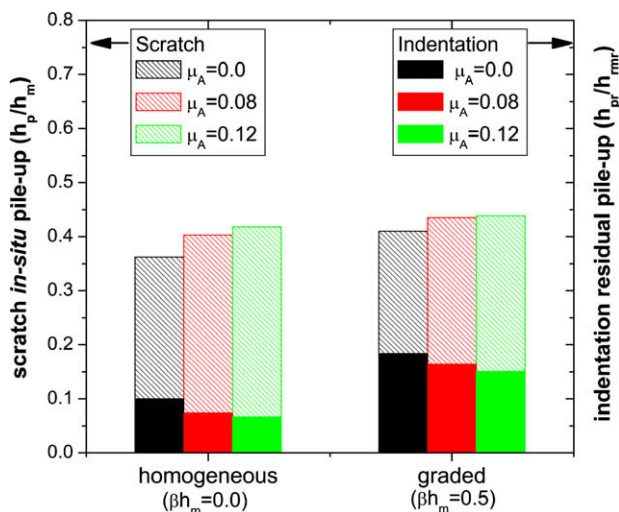


Fig. 10. Effect of friction on the pile-up height for steady-state scratch and indentation. Friction causes an increase in the pile-up in the scratch test shown by the shaded bars. However, during indentation, pile-up decreases with an increase in friction, as shown above by the solid bars.

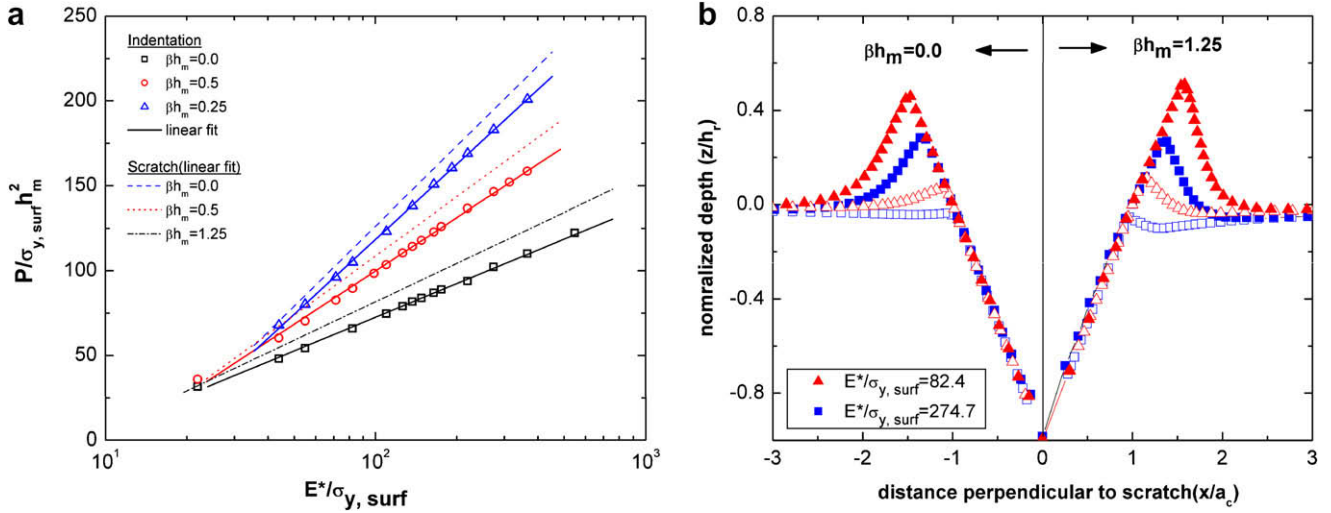


Fig. 11. Comparison of the indentation and the scratch test through (a) loading and (b) pile-up response (open symbols are for indentation and filled symbols are for scratch). For constant depth scratch, the indentation load is less than the scratch load, whereas the trends with increasing plasticity and gradient remain the same. The pile-up behavior in indentation is significantly less than that in scratch, both for the homogeneous and graded material.

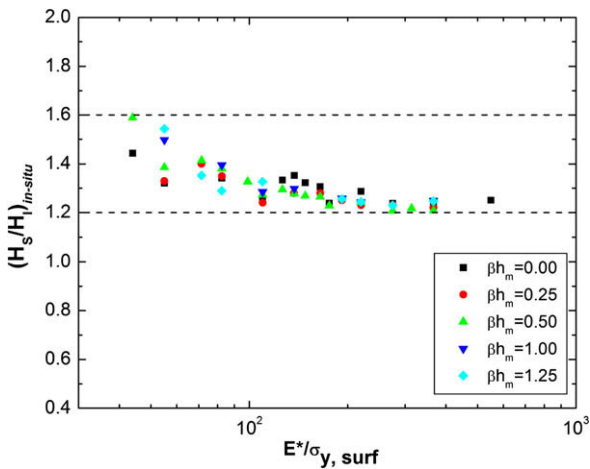


Fig. 12. Ratio of true hardness of scratch and indentation. Overall, the value lies between 1.6 and 1.2 for the material property and the gradients considered. The hardness ratio decreases with increasing plasticity, showing the increasing effect of pile-up behavior.

4.6.1. Pile-up response

The selected functional form for constructing the  $\Pi_1$  function is given by

$$\Pi_1 = \frac{h_p}{h_m} = A_h - B_h \ln \left( \frac{E^*}{\sigma_{y,surf}} + C_h \right), \quad (14)$$

where the coefficients  $A_h$ ,  $B_h$  and  $C_h$  are functions of  $A = \beta h_m$  as given below

$$A_h = 0.0955\Lambda^2 - 0.2919\Lambda - 0.0721$$

$$B_h = 0.0392\Lambda^2 - 0.088\Lambda - 0.095$$

$$C_h = -5.0763\Lambda^2 + 8.1296\Lambda - 36.087$$

Note that the pile-up response obtained from simulations is associated with mesh sensitivity (as discussed in Section 4.3). Despite this limitation, the constructed dimensionless function  $\Pi_1$  captures well both the low sensitivity of pile-up to material gradient and its stronger sensitivity to elastic-plastic ratio, as shown earlier in Fig. 5a.

4.6.2. Load response

The selected functional form for constructing the  $\Pi_2$  function is given by

$$\Pi_2 = \frac{P}{\sigma_{y,surf} h_m^2} = A_P + B_P \ln \left( \frac{E^*}{\sigma_{y,surf}} \right), \quad (15)$$

where the fitting coefficients  $A_P$  and  $B_P$  are

$$A_P = 24.91\Lambda^2 - 123.01\Lambda - 70.211$$

$$B_P = -10.815\Lambda^2 + 41.26\Lambda + 32.909$$

These predictions of the  $\Pi_2$  function with respect to the FEM simulation data are shown earlier in Fig. 6a. The constructed dimensionless function fits all the computational results very well.

4.6.3. Apparent friction coefficient

The selected functional form for constructing the  $\Pi_3$  function is given by

$$\Pi_3 = \frac{F_T}{P} = A_\mu + B_\mu (1/\Gamma)^{C_\mu}, \quad (16)$$

where  $\Gamma = \frac{E^*}{\sigma_{y,surf}}$ , and the coefficients  $A_\mu$ ,  $B_\mu$  and  $C_\mu$  are

$$A_\mu = 0.0169\Lambda^2 - 0.017\Lambda + 0.2427$$

$$B_\mu = 0.4507\Lambda^2 - 0.8504\Lambda - 0.883$$

$$C_\mu = -0.0731\Lambda^2 + 0.0265\Lambda + 0.688$$

The predictions of the  $\Pi_3$  function are shown earlier in Fig. 8, again fitting all the computational results very well.

Within the parameter space studied in the FEM analysis, the above equations together with the hardness

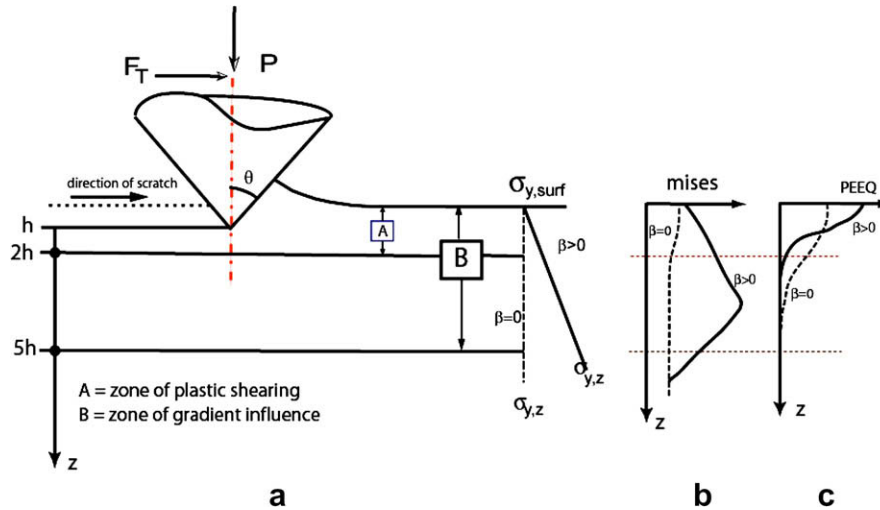


Fig. 13. Schematic of the gradient influence ( $\beta > 0$ ) on material response under sliding. As shown, zone “A” denotes the zone of plastic shearing and zone “B” denotes zone of gradient influence.

equation derived earlier, provide the ability to predict the scratch response ( $H_s$ ,  $P$ ,  $h_p$ ,  $\mu_{app}$ ) from known material properties ( $E^*$ ,  $\sigma_{y,surf}$ ,  $\beta$ ,  $h_m$ ,  $n$ ,  $\mu_a$ ). Therefore, this set of closed-form equations enables the “forward” predictive capability without additional FEM simulations within the parameter space. In addition, using Eq. (16) and the experimentally obtained apparent friction coefficient ( $\mu_{app,exp}$ ), the value of interfacial adhesive friction can be obtained as a first approximation from

$$\mu_a = \mu_{app,exp} - \Pi_3 \quad (17)$$

## 5. Concluding remarks

This work has established the first systematic methodology to quantify the steady-state frictional sliding response for a plastically graded material. Specifically, the effect of linear gradient in yield stress on the frictional sliding response is examined through parametric FEM computation of the instrumented scratch test. The basic conclusions of the present study are as follows.

1. A positive gradient in yield strength is observed to affect both the load carrying capacity of the material and its pile-up response.
  - The pile-up increases with the presence of lower gradients, gradually changing to a decreasing trend at steeper values of gradients. The underlying mechanism is rationalized through the localized nature of plastic straining (see Fig. 13c where PEEQ denotes equivalent plastic strains), which leads to a strong dependence of the pile-up on the near-surface properties (zone A in Fig. 13a).
  - The presence of a positive plastic gradient causes an increase in the load capacity for all material properties considered here. In contrast to the pile-up, the load response is dominated by the bulk properties

of the material, with the zone of influence being approximately five times the scratch depth (zone B in Fig. 13a). More important is the effect of gradient on the redistribution of von Mises stresses such that the peak values shift below the surface, thus improving the surface resistance to damage evolution (Fig. 13b).

2. The main differences of the effect of plastic gradient, as compared to the frictional sliding response of homogeneous materials, are identified as follows (also see Fig. 13a and 13b, where the dashed lines denote response of the homogeneous samples).
  - Consistent with earlier studies on homogeneous materials [25–27], strong effects of elastic-plastic ratio ( $E^*/\sigma_{y,surf}$ ) and strain-hardening exponent ( $n$ ) are observed on the pile-up response. In contrast, presence of the gradient shows a much smaller effect on the pile-up value.
  - For a given ratio of  $E^*/\sigma_{y,surf}$ , the increase in load capacity with strain-hardening is associated with higher stresses on and near the surface while the presence of a positive plastic gradient causes the highly stressed zone to be redistributed below surface (Fig. 13b).
3. The hardness of the material increases with increasing positive gradient. Using a representative strain of 33.6% [25,27], a “representative depth” of 0.65 times the scratch depth is identified; where the hardness curves for different plasticity gradients can be expressed independent of the plasticity gradient (Fig. 7b).
4. For a given elastic-plastic property, an increasing positive gradient is observed to decrease total apparent friction through a reduction in the ploughing coefficient (Fig. 8). This aspect of the gradient effect is significant in potential tribological applications of graded materials.

5. The contact-load-bearing capacity of plastically graded materials follows the similar trend in behavior during indentation and scratch, with the value being approximately 10% higher in scratch than during indentation (Fig. 11a). However, significant differences between the pile-up and the friction response are observed. In particular, an increase in interfacial friction is found to cause an increase in pile-up during scratch, while it causes a decrease in the pile-up during indentation. Overall, the ratio between *in-situ* measures of the two hardness measures is found to be within 1.2 to 1.6 for all properties and gradients considered in this analysis.
6. Dimensionless functions are constructed to predict aspects of the forward problem of the steady-state sliding response for PGMs currently investigated. These functions have important practical implications, as for example in the design of grain-size graded nanocrystalline materials, which are characterized by a low strain hardening. In addition, this approach provides the foundation for further extension to other material hardenings and indenter angles.

Based on these new developments, the basic guidelines for tailoring surfaces through controlled yield strength gradient design can be summarized as follows. (a) It is sufficient to have plasticity gradients confined within five times the expected scratch depth so as to influence frictional sliding response significantly; (b) steeper gradients can be used to decrease the material removal response; (c) for a given material, the choice between introducing gradients in yield strength versus increasing the surface strain-hardening to improve contact-damage resistance can be made based on the fact that while the gradient in material strength causes an increase in the load capacity together with a redistribution of peak stresses below surface, no significant improvement in the pile-up response can be obtained.

Thus, while the significance of plastic property gradient as an important tool in the design of functional materials was recognized earlier, the present study identifies practical guidelines for the design and for the understanding of the mechanics of deformation in these materials. In summary, this study addresses some of the fundamental questions related to the mechanism and design of plastically graded surfaces for sliding contact; provides a quantitative framework to predict sliding response through the constructed closed-form functions; identifies important differences between the homogenous and graded material response; and provides a systematic methodology to design and evaluate nanocrystalline materials with controlled gradient in grain-size as validated in our related experimental work [61]. It is known from prior work [62] that the equivalence between the mechanics of contact and the mechanics of failure imply the carryover of many of the general trends established in this study on frictional sliding at surfaces to situations involving failure progression and damage tolerance.

## Acknowledgements

The authors would like to acknowledge the financial support of the Defense University Research Initiative on Nano Technology (DURINT) which is funded at MIT by ONR under Grant N00014-01-1-0808 and by the ONR Grant N00014-08-1-0510, as well as a research grant provided by Schlumberger Limited.

## References

- [1] Beste U, Hartzell T, Engqvist H, Axen N. Surface damage on cemented carbide rock-drill buttons. *Wear* 2001;249:324.
- [2] Bhushan B. Nanotribology and nanomechanics of MEMS/NEMS and BioMEMS/BioNEMS materials and devices. *Microelectron Eng* 2007;84:387.
- [3] Boer de MP, Mayer TM. Tribology of MEMS. *MRS Bull* 2001;26:302.
- [4] Sasaki M, Hirai T. Fabrication and Properties of Functionally Graded Materials. *Nippon Seramikku Kyokai Gakujutsu Ronbunshi – J Ceram Soc Jpn* 1991;99:1002.
- [5] Kesler O, Matejcek J, Sampath S, et al. Measurement of residual stress in plasma-sprayed metallic, ceramic and composite coatings. *Mater. Sci. Eng. A* 1998;257:215.
- [6] Suresh S. Graded materials for resistance to contact deformation and damage. *Science* 2001;292:2447.
- [7] Giannakopoulos AE, Suresh S. Indentation of solids with gradients in elastic properties: 1. Point force. 2. Axisymmetric Indenters. *Int J Solids Struct* 1997;34:2357.
- [8] Suresh S, Giannakopoulos AE, Olsson M. Elastoplastic analysis of thermal cycling: layered materials with sharp interfaces. *J Mech Phys Solids* 1994;42:979.
- [9] Jitcharoen J, Padtare NP, Giannakopoulos AE, Suresh S. Hertzian-crack suppression in ceramics with elastic-modulus-graded surfaces. *J Am Ceram Soc* 1998;81:2301.
- [10] Suresh S, Olsson M, Giannakopoulos AE, Padtare NP, Jitcharoen J. Engineering the resistance to sliding-contact damage through controlled gradients in elastic properties at contact surfaces. *Acta Mater* 1999;47:3915.
- [11] Giannakopoulos AE. Indentation of plastically graded substrates by sharp indentors. *Int J Solids Struct* 2002;39:2495.
- [12] Cao YP, Lu J. A new scheme for computational modeling of conical indentation in plastically graded materials. *J Mater Res* 2004;19:1703.
- [13] Choi IS, Dao M, Suresh S. Mechanics of indentation of plastically graded materials. I. Analysis. *J Mech Phys Solids* 2008;56:157.
- [14] Choi IS, Detor AJ, Schwaiger R, Dao M, Schuh CA, Suresh S. Mechanics of Indentation of plastically graded materials: II. Experiment on nanocrystalline alloys with grain size gradients. *J Mech Phys Solids* 2008;56:172.
- [15] Hall EO. The Deformation and Ageing of mild steel: III-Discussion of Results. *Proc Phy Soc London, Sect B* 1951;64:747.
- [16] Petch N. The Cleavage Strength of polycrystals. *J Iron Steel Ins London* 1953;174:25.
- [17] Gleiter H. Nanostructured materials. *Adv Mater* 1992;4:474.
- [18] Kumar KS, Van Swygenhoven H, Suresh S. Mechanical behavior of nanocrystalline metals and alloys. *Acta Mater* 2003;51:5743.
- [19] Dao M, Lu L, Asaro RJ, De Hosson JTM, Ma E. Toward a quantitative understanding of mechanical behavior of nanocrystalline metals. *Acta Mater* 2007;55:4041.
- [20] Detor AJ, Schuh CA. Tailoring and patterning the grain size of nanocrystalline alloys. *Acta Mater* 2007;55:371.
- [21] Pender DC, Padtare NP, Giannakopoulos AE, Suresh S. Gradients in elastic modulus for improved contact-damage resistance. Part I: the silicon nitride-oxy-nitride glass system. *Acta Mater* 2001;49:3255.
- [22] Bulsara V, Chandrasekar S, Farris NF. Mechanical testing and evaluation, vol. 8: scratch testing, ASM International, 1992.

- [23] Jacobsson S, Olsson M, Hedenqvist P, Vingsbo O. Friction, Lubrication, and Wear Technology: ASM International; 1992.
- [24] Williams J. Analytical models of scratch hardness. *Tribol Int* 1996;29:675.
- [25] Bellemare S, Dao M, Suresh S. The frictional sliding response of elasto-plastic materials in contact with a conical indenter. *Int J Solids Struct* 2007;44:1970.
- [26] Wredenberg F, Larsson PL. On the numerics and correlation of scratch testing. Stockholm, Sweden: Royal Institute of Technology; 2007.
- [27] Bellemare S, Dao M, Suresh S. Effects of mechanical properties and surface on elastic–plastic sliding contact. *Mech Mater* 2008;40:206.
- [28] Mohs F. Treatise on mineralogy [Haidinger W. Trans.]. Edinburgh: Constable; 1825 [Grundriss der mineralogie, Original work published 1824].
- [29] Brinell J. II Congress Int. d. Methodes d'essai. *Iron Steel Inst* 1900;59:243.
- [30] Meyer E, Zeits D. *Vereines Deutsch. Ingenieure* 1908;52:645.
- [31] Tabor D. Physical meaning of indentation and scratch hardness. *Br J Appl Phys* 1956;7:159.
- [32] O'Neill H. Hardness measurement of metals and alloys. Chapman & Hall; 1967.
- [33] Brookes CA. Scratch and indentation hardness of crystals. *Philos Mag A* 1981;43:529.
- [34] Buttery T, Archard J. Grinding and abrasive wear. *Proc Inst Mech Eng* 1971;185:537.
- [35] Oliver WC, Pharr GM. An improved technique for determining hardness and elastic-modulus using load and displacement sensing indentation experiments. *J Mater Res* 1992;7:1564.
- [36] Dao M, Chollacoop N, Van Vliet KJ, Venkatesh TA, Suresh S. Computational modeling of the forward and reverse problems in instrumented sharp indentation. *Acta Mater* 2001;49:3899.
- [37] Gouldstone A, Chollacoop N, Dao M, Li J, Minor A. Indentation across size scales and disciplines: recent developments in experimentation and modelling. *Acta Mater* 2007;55:4015.
- [38] Hamilton G, Goodman L. The stress field created by a circular sliding contact. *J Appl Mech* 1966;33:371.
- [39] Challen JM, Oxley PLB. Slip line field analysis of the transition from local asperity contact to full contact in metallic sliding friction. *Wear* 1984;100:171.
- [40] Mulhearn TO, Samuels LE. Abrasion of metals – model of process. *Wear* 1962;5:478.
- [41] Black A, Kopalinsky E, Oxley P. An investigation of the different regimes of deformation which can occur when a hard wedge slides over a soft surface. the influence of wedge angle, lubrication and prior plastic working of the surface. *Wear* 1988;123:97.
- [42] Torrance AA. Approximate model of abrasive cutting. *Wear* 1987;118:217.
- [43] Scrutton R, Yousef N. Action of the build-up when scraping with rough conical tools. *Wear* 1970;15:411.
- [44] Childs THC, Walters MH. On the approximate numerical analysis of slip-line fields. *Int J Mech Sci* 1985;27:823.
- [45] Gilormini P, Felder E. Theoretical and experimental study of the ploughing of a rigid-plastic semi-infinite body by a rigid pyramidal indenter. *Wear* 1983;88:195.
- [46] Williams J, Xie Y. The generation of wear surfaces. *J Phys D Appl Phys* 1992;25:A158.
- [47] Bowden F, Tabor D. The friction and lubrication of solids. Clarendon Press; 1986.
- [48] Tabor D. The hardness of solids. *Rev Phys Technol* 1970;1:145.
- [49] Goddard J, Wilman H. A theory of friction and wear during the abrasion of metals. *Wear* 1962;5:114.
- [50] Johnson KL. Correlation of indentation experiments. *J Mech Phys Solids* 1970;18:115.
- [51] Bishop R, Hill R, Mott N. The theory of indentation and hardness. *Proc Roy Soc* 1945;57:147.
- [52] Marsh D. Plastic flow in glass. *Proc Roy Soc Lond A Math Phys Sci* 1964;279:420.
- [53] Hirst W, Howse M. The indentation of materials by wedges. *Proc Roy Soc Lond A Math Phys Sci* 1969;311:429.
- [54] Felder E, Bucaille JL. Mechanical analysis of the scratching of metals and polymers with conical indenters at moderate and large strains. *Tribol Int* 2006;39:70.
- [55] Bucaille JL, Felder E, Hochstetter G. Mechanical analysis of the scratch test on elastic and perfectly plastic materials with the three-dimensional finite element modeling. *Wear* 2001;249:422.
- [56] Subhash G, Zhang W. Investigation of the overall friction coefficient in single-pass scratch test. *Wear* 2002;252:123.
- [57] Johnson KL. Contact mechanics. London: Cambridge University Press; 1985.
- [58] Bolshakov A, Pharr G. Influences of pileup on the measurement of mechanical properties by load and depth sensing indentation techniques. *J Mater Res* 1998;13:1049.
- [59] Cheng YT, Cheng CM. Scaling, dimensional analysis, and indentation measurements. *Mater Sci Eng R Rep* 2004;44:91.
- [60] Stilwell N, Tabor D. Elastic recovery of conical indentations. *Proc Phys Soc* 1961;78:169.
- [61] Prasad A. Sliding contact at plastically graded surfaces and applications to surface design. PhD Thesis. Department of Civil and Environmental Engineering, Massachusetts Institute of Technology; 2007.
- [62] Giannakopoulos AE, Lindley TC, Suresh S. Aspects of equivalence between contact mechanics and fracture mechanics: theoretical connections and a life-prediction methodology for fretting fatigue. *Acta Mater* 1998;46:2955.